

A real-space analysis of colloidal crystallization in a gravitational field at a flat bottom wall

Jacob P. Hoogenboom,^{a),b)} Peter Vergeer,^{c)} and Alfons van Blaaderen^{a)}

FOM Institute for Atomic and Molecular Physics, Kruislaan 407, 1098 SJ, Amsterdam, The Netherlands and Soft Condensed Matter, Debye Institute, Utrecht University, Princetonplein 5, 3584 CC Utrecht, The Netherlands

(Received 31 March 2003; accepted 15 May 2003)

We have studied crystallization in a system of sedimenting colloids in real space using fluorescence confocal microscopy. During sedimentation a gradient in particle concentration develops at the bottom of the sample container. The presence of the lower boundary wall induces layering in the liquid and, upon increasing sediment thickness, crystallization occurs in these liquid layers. Crystallization in the first layer was found to proceed via a first-order transition. The formation of small crystal nuclei in this layer induced epitaxial crystal growth in the second layer on top of these two-dimensional crystal planes, which resulted in both layers undergoing the phase transition simultaneously. The critical osmotic pressures for crystallization at a flat wall as well as for epitaxial crystallization on an already crystallized layer were determined. The nucleation-and-growth mechanism led to a polycrystalline end state. Due to this polycrystallinity we could not determine whether the crystallization process involved an intermediate “hexatic-like” phase. Our results regarding the nature of the transition in the first two layers are in agreement with recent computer simulations [Biben, Ohnesorge, and Löwen, *Europhys. Lett.* **28**, 665 (1994)]. © 2003 American Institute of Physics. [DOI: 10.1063/1.1589737]

I. INTRODUCTION

Although freezing and melting are at the basis of many everyday phenomena, the exact nature and mechanisms underlying these phase transitions are still poorly understood and are the subject of ongoing research. This even holds for what is arguably the simplest model system in condensed matter physics, particles interacting through a hard-sphere potential. The notion that such a system can spontaneously crystallize, driven by entropy alone,^{1,2} was initially met with skepticism, but is now widely accepted.³ Nevertheless, the actual mechanism by which crystal nucleation in a supersaturated hard-sphere liquid proceeds has been only recently addressed as a consequence of developments in computational³ and experimental physics.^{4,5}

It took quite a number of years after the early work of Wood and Jacobson and Alder and Wainwright^{1,2} before the hard-sphere potential could be approximately realized in an experimental system: a dispersion of colloids. Colloids have been such an appropriate experimental realization of the hard-sphere model system for two reasons. On the one hand their interaction potential can be tuned in such a way that it spans the whole range from effective hard-sphere-like, through short-range attractive, to long-range repulsive. On the other hand, their length and time scales are easily accessible from an experimental point of view, e.g., using (light)

scattering or microscopy techniques. The development of a model system of fluorescently labeled core-shell colloids,⁶ together with the use of three-dimensional confocal microscopy^{7,8} has led to the recent experimental realization of quantitative real-space analyses of glass formation^{4,9,10} and crystal nucleation⁵ in hard-sphere systems.

In many natural and experimental systems, molecular crystal growth is influenced by impurities, which make it hard to observe pure homogeneous crystallization without special precautions. A lot of research has been done on crystallization at flat walls¹¹ both theoretically and with computer simulations as well as experimentally. The influence of a hard wall, which can be seen as the simplest external potential, on colloidal crystallization has been examined as well. In the liquid state the presence of a hard wall can already cause strong perturbations, leading to layering of the colloidal liquid¹² and eventually to prefreezing or possibly even wetting.^{13–16} These effects can be more pronounced when the wall carries a surface pattern with similar symmetry as a crystal plane, a phenomenon called colloidal epitaxy.^{15–18}

In many colloidal systems, crystallization is furthermore influenced by the presence of a second force field, namely gravity. Under the influence of gravity, colloids settle towards the bottom of their container, where, at increasing density, crystallization and subsequent crystal growth will take place. It is hard to grow colloidal crystals without sedimentation being important.^{19,20} Furthermore, the method to grow colloidal crystals through sedimentation is often used in (photonic) applications.^{17,21–25} A thorough understanding of the mechanisms of crystallization is crucial both for our understanding of colloidal crystallization in general as well as for the further development and applicability of colloidal

^{a)}Authors to whom correspondence should be addressed. Electronic mail: j.p.hoogenboom@utwente.nl; Electronic mail: a.vanblaaderen@phys.uu.nl

^{b)}Present address: Applied Optics Group, MESA⁺ Research Institute & University of Twente, P.O. Box 217, NL-7500 AE Enschede, The Netherlands.

^{c)}Currently at Chemistry of Condensed Matter group, Debye Institute, Utrecht University, Princetonplein 5, 3584 CC Utrecht, The Netherlands.

crystals in advanced applications. During sedimentation in a strong gravitational field, the formation of a layered liquid at the bottom wall will precede the formation of a crystal at the bottom of the sediment. The nature of this liquid-to-crystal transition in a one-dimensional field has been previously investigated,^{19,26} but only recently the limit of very strong field strength (gravitational length comparable to the thermal energy) has been addressed by Biben *et al.*²⁷ They showed that the first two layers of the layered liquid at the bottom wall undergo a first-order phase transition with increasing gravitational strength.

The formation of a crystalline sediment is, however, not *a priori* clear. Rather, the interplay between the particle fluxes associated with both sedimentation and crystallization is crucial for determining whether a crystalline or an amorphous sediment results. Crystal growth in a sediment of particles with a small Peclet number, i.e., the ratio between the gravitational field strength and thermal energy expressed as $Pe = (\Delta\rho)gR^4/kT$, with $\Delta\rho$ the density difference between particles and solvent, g the gravitational constant, R the particles radius, k Boltzmann's constant, and T the temperature, was examined by Davis *et al.*²⁶ Under these conditions, the gradients in the particle concentration profile are small and crystallization can be described by using local average concentrations and other thermodynamic variables. Here, the crystals grow epitaxially in a one-dimensional (1D) way. In the other extreme, at very large Peclet numbers, the Brownian motion in the direction of the external field becomes so small that this system resembles a two-dimensional (2D) system and a monolayer of colloids can crystallize. This limit can be reached not only in a gravitational field,²⁸ but also for instance by radiation pressure.²⁹ At higher volume fractions, such a high field can lead to an amorphous sediment.

Considerable research, both theoretical as well as experimental, has been performed to elucidate the mechanisms of freezing and melting in 2D model systems. As in a 2D system, true long-ranged translational order cannot exist due to a divergence in the relaxation of phonon modes; these phase transitions address the occurrence of quasi-long-ranged translational order (see, e.g., Ref. 30). In the following we will simply use the term "long-ranged order" for 2D systems as well, and assume it to be clear that in these situations we are actually dealing with quasi-long-ranged order. The Kosterlitz–Thouless–Halperin–Nelson–Young (KTHNY) theory^{31–34} predicts a two-stage melting process. In the KTHNY scenario the transition from the liquid state, characterized by both short-ranged positional and short-ranged orientational order, to the solid state with long-ranged positional and orientational order proceeds via a phase with short-ranged positional order but long-ranged orientational order. This intermediate phase is called the hexatic phase. For a system of 2D hard disks the occurrence of an intermediate hexatic phase is still unclear. Its existence has been predicted theoretically,³⁵ but computer simulations cannot rule out the possibility of a weak first-order phase transition.³⁶ For systems with an attractive interaction potential, computer simulations showed the occurrence of a stable hexatic phase,³⁷ which was confirmed experimentally.³⁸ Furthermore, the hexatic phase has been observed in 2D colloidal systems

interacting via a screened Coulomb potential,³⁹ though the occurrence of the hexatic phase may in this case be due to the presence of short-ranged attractions,³⁷ and in systems with dipole–dipole interactions.^{28,40} Only in a system of colloids interacting through a short-ranged repulsive potential was a first-order transition directly from the liquid to the solid observed.⁴¹ The various order parameters that we will use to characterize the layer-wise liquid–solid transition during particle sedimentation will include several that can distinguish the presence of an intermediate hexatic phase.

Here, we present a detailed, real-space analysis of colloidal crystallization at a wall during sedimentation of a model system of slightly charged colloidal spheres. Compared to the work of Davis *et al.*²⁶ our system has a Peclet number that is about two orders of magnitude larger. The softness of the interactions results in a (close-packed) crystal volume fraction of 0.31 after complete sedimentation, compared to ~ 0.74 for true hard spheres. The initial stage of crystal nucleation in the sediment at the bottom wall under increasing osmotic pressure during particle sedimentation will be especially addressed. Our experimental situation resembles the already-mentioned work of Biben *et al.*,²⁷ who performed Monte Carlo (MC) simulations and density functional theory (DFT) calculations on a system of hard spheres at a fixed density under increasing gravitational constant. We will compare our results directly to their work, by integrating the density profile in a mean-field way that is, however, only exact for small Peclet numbers.^{42–44} We will address these differences and their possible consequences later in this paper. In our system, the Peclet number is fairly high and we therefore give a description using 2D order parameters, similarly to the work of Biben *et al.*²⁷ and Heni and Löwen.^{15,16} Furthermore, crystallization will occur in liquid layers oriented perpendicular to the gravitational direction as layering of the colloidal liquid occurs before the point at which crystallization occurs.¹² These layers will order in their most densely packed structure, namely hexagonal planes of a close-packed crystal like the (111) face of a face-centered cubic (fcc) crystal. The fact that crystallization occurs in an already layered system raises the question whether the crystallization process in each layer can be regarded as a separate 2D process. The order parameters that will be used to probe the liquid–solid transition will enable a layer-wise (2D) analysis of the occurrence of long-ranged bond orientational and translational order, which can probe the presence of an intermediate hexatic phase.⁴⁵

II. EXPERIMENT

A. Setup and model system

Confocal microscopy was performed on a system of fluorescent silica core-shell particles to obtain three-dimensional (3D) particle coordinates.⁴ The core of the particles contained the fluorescent dye rhodamine isothiocyanate (RITC) and had a radius of approximately 100 nm. These particles have been described in detail elsewhere.⁸ In a continuous-feed seeded-growth synthesis as described by Giesche,⁴⁶ these particles were grown to a final radius of 997

nm with a polydispersity of 3.3% as measured by transmission electron microscopy. Particles were dispersed in a refractive-index matching mixture of demineralized water and glycerol (Baker, z.A grade) in a volume ratio of 1:7.18. The refractive index was measured on an Abbe refractometer (Jena 202853) and was found to be 1.4548 at a wavelength of $\lambda=589$ nm at a temperature of $T=21$ °C. Transmission spectra were taken on a spectrophotometer (Cary 5 UV-Vis-IR) and confirmed that this solution indeed showed the highest transmission at the RITC excitation and emission wavelengths (520–580 nm) as compared to other mixtures. Apart from refractive-index matching, the mixture of water and glycerol also has the advantage that due to the high viscosity (on the order of 10^2 mPa·s) the time scales for particle motion are scaled to the order of minutes, which makes a dynamical analysis of a large number of particles possible.

The bottom of the sedimentation container consisted of a 22-mm-diameter Chance no. 1 coverslip, which had been immersed in chromosulfuric acid (Merck) for 20 min and rinsed with demineralized water and ethanol (Merck, technical grade) before coating with a layer of poly(methylmethacrylate) (PMMA) to prevent particle adhesion. PMMA (950k, 4 wt% in chlorobenzene, MicroChem Corp.) was spincoated at 1000 rpm for 30 s and subsequently baked for 1 h at 170 °C. A bottomless flask with an internal diameter of 9.65 mm was glued to the PMMA-coated coverslip using silicon rubber adhesive RTV 102 (General Electric). The sedimentation container was rinsed several times with the water/glycerol mixture before being filled with 0.86 ml of dispersion with a volume fraction of $\varphi_0=0.0039$.

The suspension was left to sediment mounted on a confocal microscope (Leica TCS NT-2). During sedimentation the sample was scanned regularly. The scan field size was 100×100 μm , which was scanned with a resolution of 1024×1024 pixels. Both time series of a 2D plane in the sample, with a time interval between subsequent scans of 40 s, and stacks of 2D scans with a stepsize of 0.12 μm , were acquired.

In each 2D frame, feature coordinates were retrieved using image-analysis software similar to that described in Ref. 47, written in the programming language IDL.⁴⁸ For retrieving particle coordinates from the 3D stacks, feature coordinates from successive frames with 2D particle coordinates that belong to a single sphere's intensity profile were grouped in columns that extend in the direction perpendicular to the scan field. This intensity profile is the z component of a convolution of the point spread function (PSF) of our microscope with the spherical profile of the core particles. A Gaussian function was constructed of which the full-width-at-half-maximum was fixed at a value such that this Gaussian function mimicked the z -axis component of the convolution of the PSF with the spherical core profile. Each of the intensity profiles in the 3D data set was then fitted to this Gaussian and the position of the maximum was taken as a particle's z coordinate. The use of the high-viscosity water/glycerol mixture makes it possible to record the 3D intensity profiles without having to correct for intermediate particle diffusion. In the remainder of this section we will use a Cartesian coordinate set, with the positive z axis parallel and

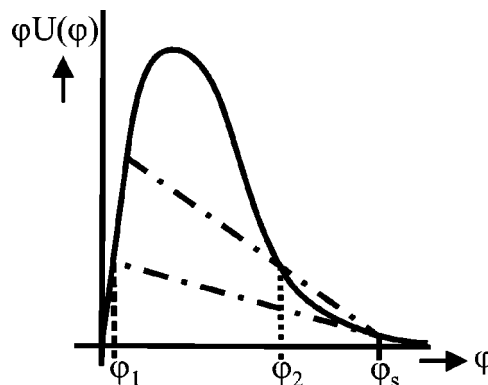


FIG. 1. Typical form of the flux curve for colloidal sedimentation. φ_s denotes the volume fraction at the top of the sediment. For initial volume fractions larger than φ_1 a fan region builds up starting from φ_2 , which at continuing sedimentation expands to higher volume fractions. For initial volume fractions smaller than φ_1 , the sedimentation flux is constant throughout the sample until the top of the sediment.

opposed to the gravitational direction, so that increasing values of z correspond to increasing height in the sample. The z direction is now along the optical axis of the confocal microscope. The error in retrieving the z coordinates with the above-mentioned procedure is ± 30 nm. The error in the lateral (xy -)coordinates is ± 10 nm.

B. Sedimentation and crystallization

The process of crystallization during sedimentation is based on a complicated interplay between the time scales associated with both processes. The time scale for sedimentation is given by the volume-fraction-dependent sedimentation velocity $U(\varphi)=U_0\cdot K(\varphi)$, where U_0 is the sedimentation velocity at infinite dilution, $U_0=2/9\cdot R^2(\Delta\rho)g/\eta$, with R , $\Delta\rho$, and g as previously defined and η as the solvent viscosity. The factor $K(\varphi)$ denotes the reduction of sedimentation velocity at higher volume fractions and can usually be well described by $K(\varphi)=(1-\varphi)^n$, where for instance for hard-spheres $n=6.6$.¹⁹

In Fig. 1 the typical form of the flux curve $\varphi\cdot U(\varphi)$ is given. The initial volume fraction φ_0 gives rise to a constant sedimentation flux $\varphi_0\cdot U(\varphi_0)$. At the bottom of the container the sediment will be formed at a volume fraction denoted in Fig. 1 by φ_s . For relatively large initial volume fractions, $\varphi_0>\varphi_1$ with φ_1 on the order of 10^{-2} , the sedimentation flux of particles, $\varphi_0\cdot U(\varphi_0)$, is larger than the maximum possible flux for a volume fraction of φ_2 and higher.¹⁹ When a volume fraction of φ_2 is reached during sedimentation, there will be a build-up of particles in a so-called fan. The fan constitutes a transition region where the volume fraction smoothly varies with depth from φ_2 to φ_s . With ongoing sedimentation the fan region will expand to higher volume fractions. In this case the flux of particles into the sediment is given by the sedimentation flux at the bottom of the fan, which, in order to yield a crystalline sediment, has to be equal to or smaller than the particle flux associated with the maximum rate of crystal growth. Under these circumstances there is a maximum sphere radius, and thus a maximum

Peclet number, above which crystallization in the sediment is prohibited by too high a sedimentation flux and an amorphous sediment results, as was experimentally verified by Davis and co-workers.²⁶ In order to be able to match the sedimentation and crystal growth fluxes, we thus have to have an initial volume fraction where the flux associated with this φ_0 is the rate-limiting step anywhere in the sample. This means that $\varphi_0 < \varphi_1$ in Fig. 1 and thus $\varphi_0 < 0.01$. Under these circumstances $K(\varphi_0) \approx 1$ and the time scale for sedimentation is determined by U_0 .

Now, we define the time scale associated with the flux of particles during sedimentation, t_{sed} , as the average time it takes before one particle sediments through an area R^2 . This

time scale depends on the initial volume fraction, and is given by $t_{\text{sed}} = R/(\varphi_0 \cdot U_0) \sim \eta/(\varphi_0(\Delta\rho)gR)$. If we now scale this t_{sed} to the typical time scale for diffusion $t_D = R^2/D_0$, i.e., the time it takes for a particle to diffuse a distance R , where $D_0 = kT/(6\pi\eta R)$, and use the Peclet number, we find $t_{\text{sed}}/t_D = 1/(\varphi_0 \cdot \text{Pe})$. For the system given above, with an initial volume fraction of $\varphi_0 = 0.0039$, we have $1/(\varphi_0 \cdot \text{Pe}) = 2.5 \times 10^3$.

C. Data analysis and order parameters

For each 3D coordinate set the linear number density, as a function of height in the sample, was calculated by integrating over the lateral (xy -)coordinates

$$\rho_z = \frac{\int_{z-(\Delta z/2)}^{z+(\Delta z/2)} \int \int \sum_{i=1}^N \delta(x-x_i) \delta(y-y_i) \delta(z'-z_i) dx dy dz'}{\Delta z \cdot \int \int dx dy} \quad (1)$$

Here, x_0 , y_0 , and z_0 denote the particle coordinates, and a uniform bin size of $\Delta z = 40$ nm was chosen. The position of the first maximum in the laterally integrated density profile was taken as $z=0$. The total number of particles in the sediment was retrieved by integrating over the z direction. As we will see in the Results section, the overall volume fraction was low enough to ensure ρ_z decaying to almost zero, corresponding to the very low φ_0 , so that both sediment thickness as well as the integration over z are well defined. The total number of particles in the sediment was found to increase linearly with time, as would be expected. The evolution of the order parameters that we will define below will depend on the evolution of the concentration profile in the sediment. The build-up of the concentration at the bottom of the sample leads to an increased gravitational pressure on the particles in the sediment. This gravitational pressure is balanced by an osmotic pressure gradient that can be directly retrieved from the instantaneous concentration profile⁴²

$$\Pi = m_b g \int_z^h \rho_{z'} dz' \quad (2)$$

The osmotic pressure at the bottom of the sample is thus directly related to the thickness of the sediment. It should be noted, however, that this mean-field approach is only exact for small Peclet numbers. We now express the sediment thickness in terms of an equivalent number of crystal layers by scaling the total number of particles in the sediment with the number of particles in a single crystal layer at the end of our experiment, 263 h after homogenization of the sample

$$N = \frac{\int \int \int \sum_i \delta(x-x_i) \delta(y-y_i) \delta(z'-z_i) dx dy dz'}{\int_{z=-0.5}^{0.5} \int \int \sum_i \delta(x-x_i) \delta(y-y_i) \delta(z'-z_i) dx dy dz' |_{t=263 \text{ hours}}} \quad (3)$$

The number of crystal layers after 263 h was $N=21$. As a comparison, all data reported below fall in the time interval from 90 to 150 h after the start of the experiment, which gives a number of layers between 8 and 13. Expressing the sediment thickness in N has the advantage that this quantity is experimentally well defined and that it can be directly related to the (mean-field) osmotic pressure at the bottom of the sample using Eqs. (1) and (2).

On the basis of the laterally integrated density profile we can see the onset of layering in the sample at the bottom wall. When layering occurs, particles can be assigned to belong to these 2D layers defined by the minima in ρ_z . Recently, Heni and Löwen suggested the use of these minima as a robust order parameter for layer-wise crystallization.¹⁶ Furthermore, it was shown in the work of Biben *et al.* that the crystallization transition in a suspension close to a hard wall under increasing gravitational field strength occurs through a

discontinuous jump to zero in the interlayer density.²⁷ As this implies that the number of particles confined to this layer also increases discontinuously, this jump would imply that the crystallization transition is of first order if judged as a 2D transition.

Furthermore, for each layer both orientational and translational order can be probed. As we expect each layer to crystallize in hexagonal symmetry, the 2D local hexagonal bond orientational order parameter for each single particle in a specific layer was calculated⁴⁵

$$\psi_6(r_j) = \frac{1}{N_b} \sum_k \exp(i6\theta(r_{jk})), \quad (4)$$

where the summation k runs over all, in total N_b , neighboring particles of particle j , and the angle θ is the angle that the bond vector between particles j and k makes with an arbitrary

fixed reference axis. In this equation, as in all the following equations for layer-wise order parameters, we denote all 2D coordinates in a layer with $r=r(x,y)$. With the definition given above, $\psi_6=1$ for a lattice with hexagonal symmetry. The distribution of neighbors to every particle is found using a Delaunay triangulation, from which the Voronoi polygon can be constructed. A Voronoi polygon is defined as the area around a particle that is closer to that particle than to any other particles; thus, the construction of the Voronoi polygon is similar to the Wigner–Seitz cell used in solid-state physics. With this local order parameter, both its layer-wise average can be evaluated as well as the corresponding correlation function $g_6(r)$

$$g_6(r) = \frac{\langle 2 \sum_{i=1}^{N-1} \psi_6^*(\mathbf{r}') \delta(\mathbf{r}' - \mathbf{r}_i) \sum_{j=i+1}^N \psi_6(\mathbf{r}'') \delta(\mathbf{r}'' - \mathbf{r}_j) \rangle}{\langle 2 \sum_{i=1}^{N-1} \delta(\mathbf{r}' - \mathbf{r}_i) \sum_{j=i+1}^N \delta(\mathbf{r}'' - \mathbf{r}_j) \rangle}, \quad (5)$$

where $r=|\mathbf{r}' - \mathbf{r}''|$. The denominator in Eq. (5) is related to the translational order correlation function, or radial distribution function, defined by

$$g(r) = \frac{1}{\rho^2} \left\langle 2 \sum_{i=1}^{N-1} \delta(\mathbf{r}' - \mathbf{r}_i) \sum_{j=i+1}^N \delta(\mathbf{r}'' - \mathbf{r}_j) \right\rangle, \quad (6)$$

with $i \neq j$. For a 2D system the occurrence of an intermediate hexatic phase can be probed by determining the envelope function of the decay of both these correlation functions. In the liquid state both correlation functions decay to zero exponentially. For the short-ranged translational order and quasi-long-ranged bond orientational order of the hexatic state the envelope function of $g_6(r)$ decays to a nonzero value with power-law dependence, while for $g(r)$ the decay is still exponentially to zero. In the crystalline end state the decay of both functions proceed algebraically to a nonzero value.⁴⁵

Apart from these static criteria, dynamical criteria also can be used to probe a liquid–solid transition.^{49,50} Here, we will carry out a mobility analysis per layer as described by Hurley and Harrowell⁵¹ in order to visualize kinetic heterogeneities consisting of relatively slowly diffusing, “caged” particles on the one hand and faster diffusing particles on the other hand. Furthermore, we will evaluate the behavior of the long-time self-diffusion coefficient D_l^s

$$D_l^s = \lim_{t \rightarrow \infty} \frac{1}{4t} \langle (r(t) - r(0))^2 \rangle, \quad (7)$$

which should decay towards zero upon crystallization. The behavior of the long-time self-diffusion coefficient can be used as a separate order parameter using the Löwen–Palberg–Simon criterion.^{49,52} Their criterion states that the ratio of the long-time and short-time self-diffusion coefficients reaches a uniform value of 0.1 upon crystallization. As the short-time self-diffusion coefficient can be assumed to stay constant during the phase transition, a sharp decay of D_l^s indicates a similar behavior for this order parameter.

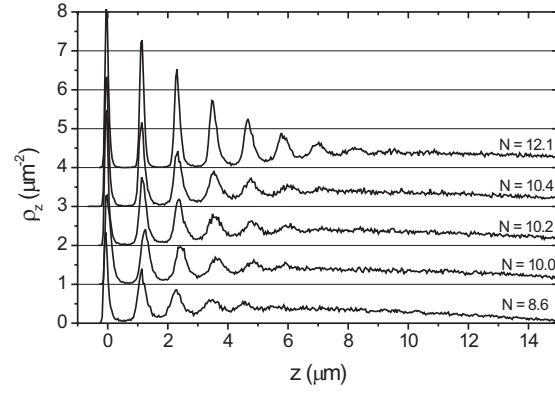


FIG. 2. Laterally integrated density profiles as a function of sediment thickness. Profiles for different values of N have been shifted by 1 for clarity.

III. RESULTS AND DISCUSSION

A. Layering and crystallization

As a start of our analysis the laterally integrated density profile ρ_z was calculated for each of our 3D coordinate sets. Several density profiles at different stages of the sedimentation process are shown in Fig. 2. As can be seen, all profiles start with a sharp peak at $z=0$ due to the presence of the bottom container wall. The exact position of the zero on the z axis has been chosen to coincide with the position of the first maximum in the density profile, as the exact position of the wall surface was not accurately retrievable from these data sets. With increasing z the density profile goes through a minimum and shows several oscillations with decreasing peak height and increasing peak width. This shows the layering at the bottom of the suspension due to the presence of the bottom container wall.¹² The oscillations in the density profiles are followed by a smooth, almost linear decay to zero. The density profiles actually decay to essentially zero due to the fact that a very low initial volume fraction of $\varphi_0 = 0.0039$ was used, which makes the sediment thickness, N , well defined. This furthermore allows for a gradual increase of the osmotic pressure.

With increasing sediment thickness, the range of oscillations increases and the first peaks in the profile become sharper. The minimum in between the first two peaks falls to zero from $N=10.2$ to $N=10.4$, and the width of this mini-

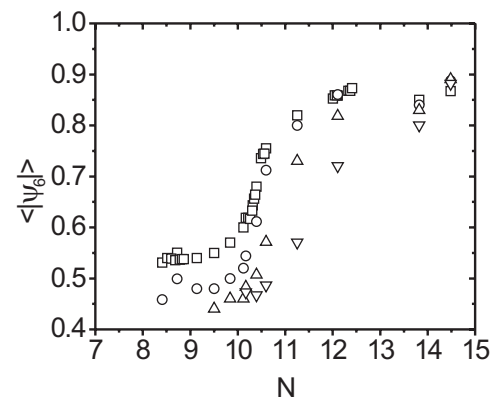


FIG. 3. The layer-wise averaged local bond order parameter ψ_6 for the first four layers indicated with squares for layer one, circles for layer two, up-triangles for layer three, and down-triangles for layer four.

TABLE I. Sediment thickness and osmotic pressures for the liquid–crystal transition in consecutive layers together with simulation results (Ref. 27) for the transition regions for these layers. The simulation results are expressed in the parameter α that probes the strength of the gravitational field relative to kT . The corresponding osmotic pressures calculated for the experimental system based on these values are given as well.

Layer	This research		Simulation results			
	N	Π (10^{-2} Nm^{-2})	α_{start}	α_{end}	Π_{start} (10^{-2} Nm^{-2})	Π_{end} (10^{-2} Nm^{-2})
1	10.4	2.36	2.50	2.75	2.17	2.39
2	10.5	2.13	2.50	2.75	1.59	1.74
3	11.0	2.01	2.50	3.30	1.00	1.32
4	11.9	1.98	3.25		0.53	

imum becomes broader. A similar process can be seen for the second minimum at higher N . We will analyze the relative depth of these minima as an order parameter below. Note that all peaks are asymmetric with a sharp, almost delta-peak-like rise followed by a slower decay to the minimum. This is most clearly visible for the first two peaks, and becomes more pronounced for higher peaks at increasing N . For the first peak this asymmetry is due to the presence of the bottom wall, but its influence remains visible for further peaks, even when the first few layers have crystallized at $N = 12.1$. This asymmetry is solely due to the presence of the wall, as this can also be seen in simulation results where no gravitational field is present. The fact that this asymmetry is so clearly reproduced in our results shows the good statistical accuracy with which these profiles are retrieved.

In Fig. 3 the evolution of the averaged local hexagonal bond order parameter, $\langle |\psi_6| \rangle$, defined in Eq. (4), is given as a function of N , for the first four layers in the sample. For the first layer $\langle |\psi_6| \rangle$ shows a sharp rise from $N = 10.2$ to $N = 10.7$, indicative of the transition to a hexagonal lattice, followed by a slower saturation towards a value of $\langle |\psi_6| \rangle \sim 0.9$. For the second layer $\langle |\psi_6| \rangle$ shows a similar evolution, starting however from a lower value, but showing a rise simultaneously with the first layer and catching up with the first layer in between $N = 10.4$ and 10.7 . For layers three and four the transition regions are qualitatively similar, but with the transition occurring at a higher, discrete value of N . Taking half the rise in $\langle |\psi_6| \rangle$, i.e., $\langle |\psi_6| \rangle \sim 0.68$, as the location of the crystallization transition, we find this transition to occur at $N = 10.4, 10.5, 11.0$, and 11.9 for layers one to four, respectively, as indicated in Table I. The corresponding osmotic pressures at these layers are also given in Table I.

In a first-order phase transition there is a discontinuous increase in the density of the crystallizing phase. A sharp rise

between the average values that can be associated with liquid and solid phases was observed for the bond orientational order parameter. We will now examine whether this phase transition is of first order. In the density profiles shown in the work of Biben *et al.*, a clear discontinuous jump in the interlayer density to zero is observed, which occurs simultaneously with an increase in order parameter. In order to test for similar behavior of the interlayer density, the relative depth of the first two minima in the density profile was determined as was suggested by Heni and Löwen.¹⁶ The density profile was integrated over a range of $0.12 \mu\text{m}$ around the minimum, and this value was taken relative to the result of integration from the start of the profile to the position of the second minimum. The results for the first and the second minimum are given in Figs. 4(a) and 4(b), respectively. Heni and Löwen calculated a direct linear correspondence of the decrease of these minimal values with the order parameter $\langle |\psi_6| \rangle$, and found the liquid–solid transition to occur when the minimal value decreased below 0.05.¹⁶ The 0.05 criterion is indicated with the dashed line in Figs. 4(a) and 4(b). For the first minimum, the relative minimal value reaches a value of 0.05 at $N = 10.2$, while for the second minimum this occurs at about $N = 10.5$. This last position is, however, much harder to pinpoint as this region is not as well sampled as for the point where the first minimum traverses the criterion of Heni and Löwen. Comparing Fig. 4(a) with Fig. 4(b), it can be seen that in the same range around the crystallization transition, the depth of the second minimum falls down from a much higher value and more drastically than does the depth of the first minimum. Apparently, layering and crystallization in the second layer proceeds much faster over a similar increase in sediment thickness than in the first layer. The reason for this is probably the difference in crystallization on a flat surface wall compared to crystallization on an already

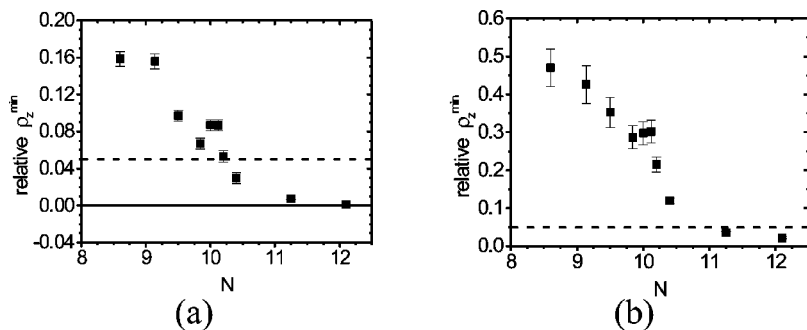


FIG. 4. The evolution of the relative depth of the minimum in ρ_z for (a) the minimum in between the first and second layer; and (b) the minimum in between the second and third layer. Note the change in scale on the vertical axis between (a) and (b). The dashed line indicates the Heni–Löwen criterion for crystallization of 0.05.

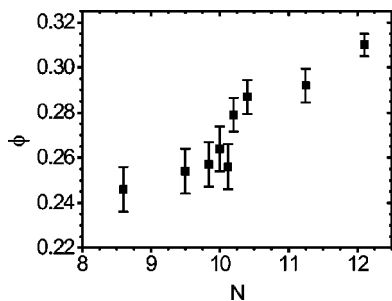


FIG. 5. The volume fraction in the first two layers above the bottom wall as a function of sediment thickness.

crystallized layer. We will come back to this point later in this section.

Based on the criterion of Heni and Löwen for the minimal interlayer density (Fig. 4), we found the transition in first and second layer to take place at $N=10.2$ and $N=10.5$, respectively. Heni and Löwen reported their criterion to coincide with an averaged value for $\langle|\psi_6|\rangle$ of $\langle|\psi_6|\rangle\sim 0.8$.¹⁶ It can be seen when comparing Fig. 4(a) and Fig. 3 that in our experimental situation, the value of $N=10.2$ found for the first layer gives $\langle|\psi_6|\rangle=0.62$. For the second layer [see Figs. 4(b) and 3] the value of $\langle|\psi_6|\rangle$ at $N=10.5$ is $\langle|\psi_6|\rangle=0.68$. Where for the first layer this seems to correspond more to the onset of crystallization as viewed from the development of $\langle|\psi_6|\rangle$, for the second layer the 5% criterion seems to correspond well with half the rise in $\langle|\psi_6|\rangle$. As both the minimal density as well as the local hexagonal order parameter show a drastic change with increasing sediment thickness, these values are very sensitive to the exact location of the criterion.

In the calculation of the relative depth of the minima in ρ_z , the density in the first two layers itself is implicitly calculated. The behavior of the minima in ρ_z seems less sensitive to experimental errors than the behavior of the density itself,⁵³ but it is still instructive to look directly at the behavior of the density in the first two layers. This density was determined by integrating the density profile from the start of the profile and dividing this by twice the layer width. The layer width was determined as the distance between the first and the second minimum. The resulting densities are given in Fig. 5. The regular increase of the density at the bottom of the sediment due to particle sedimentation is clearly interrupted by a sharp rise at the sediment thickness that was identified as the point where the first two layers crystallize. This clearly and directly indicates the first-order character of the phase transition. In order to probe the character of the liquid–crystal transition, we have also calculated the osmotic compressibility (Π/nkT) per layer as a function of sediment thickness. The phase transition was found to occur at an osmotic compressibility which was on the order of 12. The error margins were, however, too large to get a discriminating critical value for the transition at a single layer.

B. Correlation functions of local order parameters

Above, the occurrence and nature of the phase transition were examined in terms of the density in the system and the

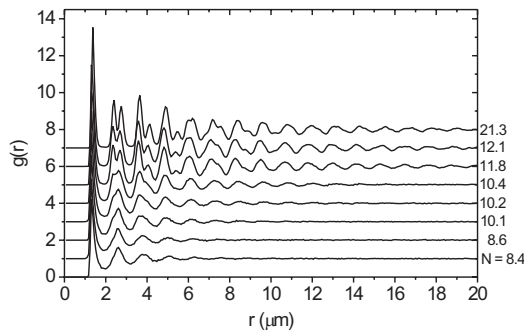


FIG. 6. Evolution of the radial distribution function $g(r)$ for particles in the first (bottom) layer for (from bottom to top) increasing values of N . Curves for different N have been shifted by 1 for clarity.

average hexagonal symmetry of neighbors surrounding a particle. Next, correlations in particle positions and in the bond orientational order will be examined. For a liquid–solid transition both types of correlations will show a transition from short-ranged to long-ranged. The nature of this transition may indicate the presence of an intermediate hexatic phase: In an intermediate hexatic phase the envelope function of $g_6(r)$ decays algebraically to a nonzero value, while the translational correlation function $g(r)$ still decays exponentially.⁴⁵ In the liquid state the decay of both functions is exponential, while in the solid phase the decay is algebraic for both functions. In Fig. 6 the radial distribution function $g(r)$ [Eq. (6)] is given for various values of N . Curves for different N have been shifted by 1 for clarity. In the first curve for $N=8.4$, we can see liquid-like behavior, with typically three or four maximums corresponding to the mean interparticle distance and integer multiples thereof, before leveling to a value of 1. Starting at $N=10.1$, it can be seen that the number of oscillations, and thus the range of correlations in particle positions, increases. The form and position of these oscillations, however, do not change and remain liquid-like. In between 10.2 and 10.4 a change in form of the correlations does show up: the slightly broadened second and third peaks in $g(r)$ both split into two distinct maximums. The positions of these maximums correspond to hexagonal lattice distances of $D\sqrt{3}$ and $2D$, and $D\sqrt{7}$ and $3D$ for the split second and third peak, respectively, where D denotes the nearest-neighbor distance in a 2D hexagonal lattice which is retrieved from the position of the first maximum in $g(r)$ at these values for N . This behavior shows the transition in the bottom-wall aligned layers from liquid-like to the order of a 2D hexagonal lattice. As was already evidenced by the rise in $\langle|\psi_6|\rangle$, the sediment consists of hexagonally stacked layers. For the curves with $N>11.8$, where the average bond orientational order parameter in the first layer had reached its saturation value (see Fig. 3), hardly any change in the positional correlations is observed anymore.

The bond orientational order correlation function $g_6(r)$ in the first layer is given in Fig. 7 for various values of the sediment thickness. In the liquid phase ($N=8.6$), $g_6(r)$ decays rapidly to zero, corresponding to the absence of long-ranged bond-order correlations in the liquid state. At the onset of crystallization (from $N=10.1$ to $N=10.4$), the rate of decay slows down and the range of correlations increases correspondingly. After $N=10.4$ the number of oscillations

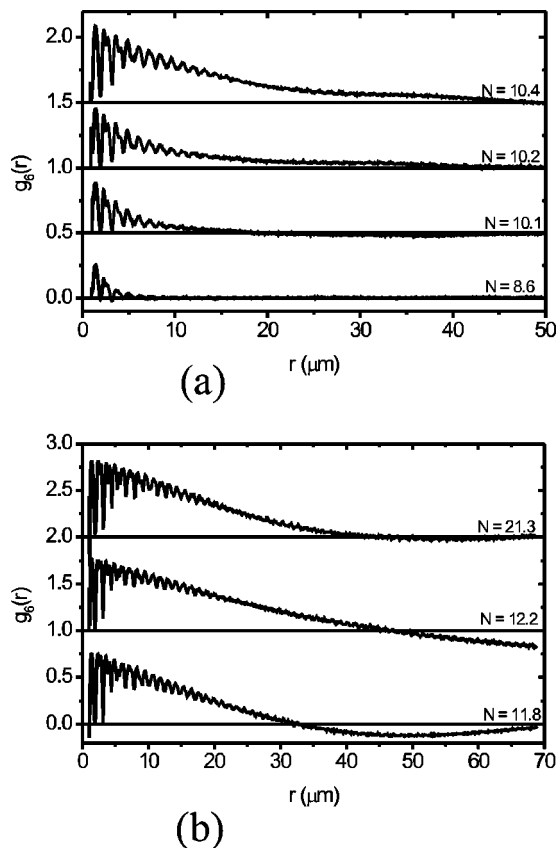


FIG. 7. The bond-order correlation function $g_6(r)$ for particles in the first (bottom) layer, for different sediment thickness in (a) the liquid phase and at the onset of crystallization, and (b) in the crystalline state. Curves in (a) have been shifted by 0.5 and curves in (b) by 1.0 for clarity. Note the different horizontal and vertical scales in (a) and (b).

increases only slightly more, until there is long-range bond-order correlation in the crystalline state at $N=11.8$ [Fig. 7(b)]. In this stage even negative correlations at a distance of 40 to 50 μm are visible. These can be attributed to the polycrystalline nature of the crystalline end state: as we will see in the next section, crystallization occurs through a nucleation-and-growth process, so that crystallites with different orientations will appear. Crystallites with only a small orientation difference will still have a possibility to rearrange, leaving the crystallites with a larger orientation difference (around 30°) that gives rise to contributions of opposite sign in Eq. (5). The onset of sign inversion of $g_6(r)$ differs for each of these curves, because the amount of crystallites per confocal image is too low and the average crystal size too small to determine the “true” range of ψ_6 to properly sample the average crystallite size. The polycrystalline nature of the end state was confirmed by confocal pictures taken at the final stage of sedimentation ($N=21.3$) as well as two months after sedimentation was completed.

As mentioned previously, we tried to fit the decay rate of the bond-order correlation function, as this might give an indication of the presence or absence of an intermediate hexatic phase. However, the decay of $g_6(r)$ was found to proceed neither exponentially nor with power-law dependence, probably because the actual behavior of the decay rate for a single crystalline domain is obscured by the finite crys-

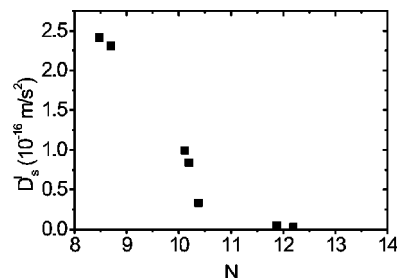


FIG. 8. The long-time self-diffusion coefficient for particles in the bottom layer as a function of sediment thickness.

tallite size that causes the sign inversion mentioned before. Although this order parameter in this specific case does not give any insight into the presence of an intermediate hexatic phase, the order parameters that were examined before indicated a single first-order transition. Furthermore, the phase transition in the first layer was found to occur at the same range of values for the sediment thickness for all order parameters, either probing orientational or translational order. Thus, based on these results we cannot rule out the occurrence of an intermediate hexatic phase, but if the liquid–crystal transition proceeds in two steps, both the liquid-to-hexatic as well as the hexatic-to-solid transition will occur very close to each other. This is, however, also what is expected for the occurrence of the hexatic phase in true 2D hard-disks systems.³⁶ When the occurrence of the 2D hexatic phase in crystallization during sedimentation is addressed in further experiments, it will also be interesting to examine this transition for the second and further layers in the sediment, as the occurrence of the hexatic phase is not ruled out by the presence of a patterned substrate potential,³³ which in this case would be provided by the colloids in the layers below. However, with increasing height in the sediment, the crystallization behavior may become less and less 2D.

C. Structure and mobility

At several stages during sedimentation, a long-time series of confocal images of the bottom layer was taken, from which the mean-squared displacements and the long-time self-diffusion coefficient [Eq. (7)] were calculated. In Fig. 8 D_s^i for the bottom layer is plotted as a function of sediment thickness N . As can be seen, the long-time self-diffusion coefficient falls off to zero sharply for $N \rightarrow 10.4$. This is in correspondence with the increase in order parameter we saw in Fig. 3 and the determination of the position of the liquid–solid transition for this first layer (Figs. 3 and 4). The decrease in D_s^i is the indication for the transition of particle motion from diffusive (with strong collective effects) to localized motions around lattice positions. In fact, as mentioned before, the behavior of the long-time self-diffusion coefficient can be used as a separate order parameter, the Löwen–Palberg–Simon criterion.^{49,52} Their criterion states that the ratio of the long-time and short-time self-diffusion coefficients reaches a uniform value of 0.1 upon crystallization. As the short-time self-diffusion coefficient can be assumed to stay constant during the phase transition because

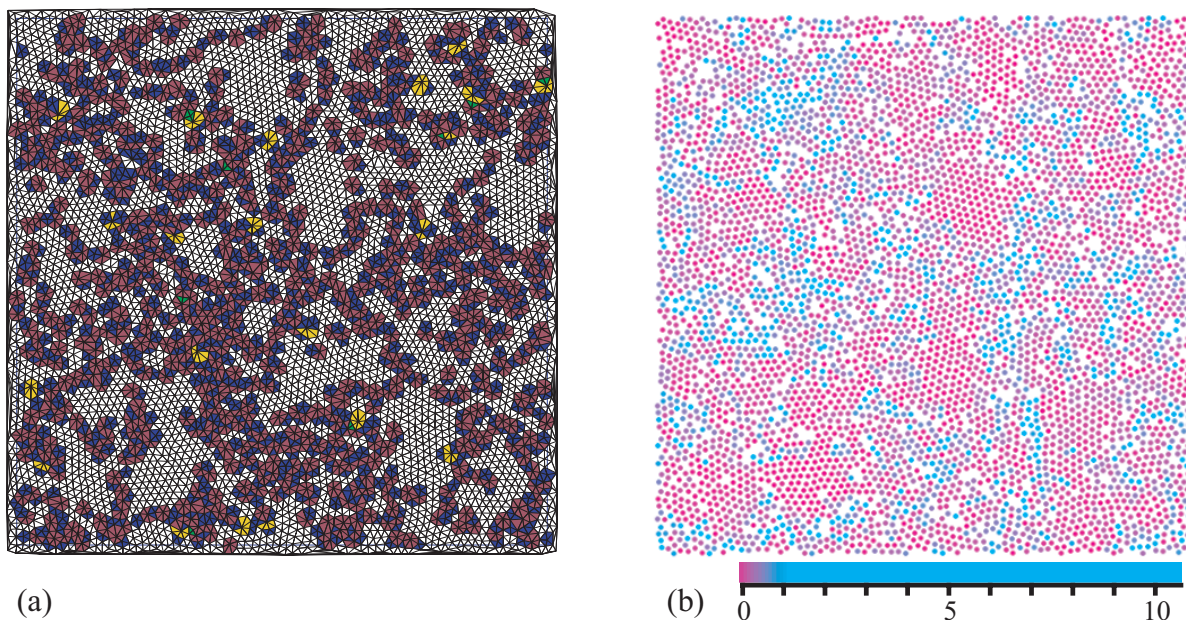


FIG. 9. (Color) (a) Delaunay triangulation for particles in the first (bottom) layer at $N=10.2$. Triangles surrounding sixfold-coordinated particles only have been left uncolored, while colored cells indicate a deviating coordination number: green for fourfold, blue for fivefold, brown for sevenfold, and yellow for eightfold-coordinated particles. (b) Snapshot of particle positions in the first layer at $N=10.2$, where particles have been colored corresponding to their mean-squared displacement over a time interval larger than the typical relaxation time. The 5% of particles undergoing the smallest displacements have been colored blue and the 5% of particles with the largest displacements have been colored in red. In between, the color changes gradually with a change in mobility, as indicated with the color table below the figure. The scale bar that belongs to the color table is in $\mu\text{m}^2/\text{h}$.

the density differences are small, the sharp decay of D_l^s shown in Fig. 8 indicates a similar behavior for this order parameter.

In order to get more insight into the actual mechanism for crystal growth, we carried out a Delaunay triangulation analysis. In Fig. 9(a) a triangulation plot of the first layer at a value of $N=10.2$ is given. Triangles have been colored based on the coordination number of the center particle, where sixfold-coordinated particles have been left uncolored. Several coherent, ordered regions can clearly be distinguished, surrounded by defect-rich areas of mostly fivefold- and sevenfold-coordinated particles. For lower values of N (not shown), clusters of sixfold-coordinated particles also appeared, but these were never larger than 5 particle diameters wide. Furthermore, a comparison of a time sequence of triangulation plots of the same area at constant $N < 10$ showed that these regions of sixfold-coordinated particles were always fluctuating in time, continuously disappearing and reappearing at other positions. This behavior is typical for a dense liquid where there is a specific correlation time that sets the time scale in which these spatial homogeneous areas can be observed.⁵¹ The larger regions in the triangulation plot shown in Fig. 9(a) were all stationary in time, and can thus be identified as small crystallites.

A similar observation can be made when examining the root-mean-squared displacements of particles. The calculated rms displacements of particles fall in a broad distribution. In Fig. 9(b) particles in the same time frame as in Fig. 9(a) are shown, but with particles colored according to their averaged mean-squared displacement over time. Particles undergoing relatively small displacements (the lower 5% of displacements) are shown in red, and the particles with the larger 5% of displacements in blue, with the color scale gradually

changing in between. A comparison of Fig. 9(b) with the triangulation plot in Fig. 9(a) shows that the positions of the particles with the lowest mobility strongly coincide with the larger regions of sixfold-coordinated particles. Thus, as might be expected, mobility decreases upon nucleation.

Figure 10(a) shows a triangulation analysis (for a different area in the sample) for $N=10.4$. At this sediment thickness, the average local bond-order parameter is now almost half its rise upon crystallization (see Fig. 3). The amount of particles that are sixfold coordinated has drastically increased, resulting in a growth of the crystallites, which are now only separated by 1 to 3 particle-diameters-wide defect lines. In the ordered regions several point defects occur. The amount of dislocations in the ordered regions is however low, and larger (or more) areas would have to be probed to get enough statistical accuracy to study the average number of defects in these crystallites.

In Figs. 10(b) to 10(d), triangulations of the same area in the three layers above are shown. As can be seen in Fig. 10(b), the second layer consists of crystallites of, on average, similar size on the same positions as in Fig. 10(a). This shows the second layer to crystallize epitaxially on top of the crystallites that nucleated in the bottom layer. In the third layer [Fig. 10(c)], ordered regions of the same size as in Fig. 10(a) can be identified. When comparing the value of $\langle |\psi_6| \rangle$ for the third layer at $N=10.4$ ($\langle |\psi_6| \rangle \approx 0.5$), we see that this is still lower than the value of $\langle |\psi_6| \rangle$ for the first layer at $N < 10$, where coherent ordered regions larger than 5 particle diameters wide did not show up yet. However, in Fig. 10(c) a few larger sixfold-coordinated regions are clearly visible, which can be identified as crystal nuclei. Indeed, it can be seen in Fig. 3 that at $N=10.4$ we are at the onset of the sharp rise in $\langle |\psi_6| \rangle$ for the third layer.

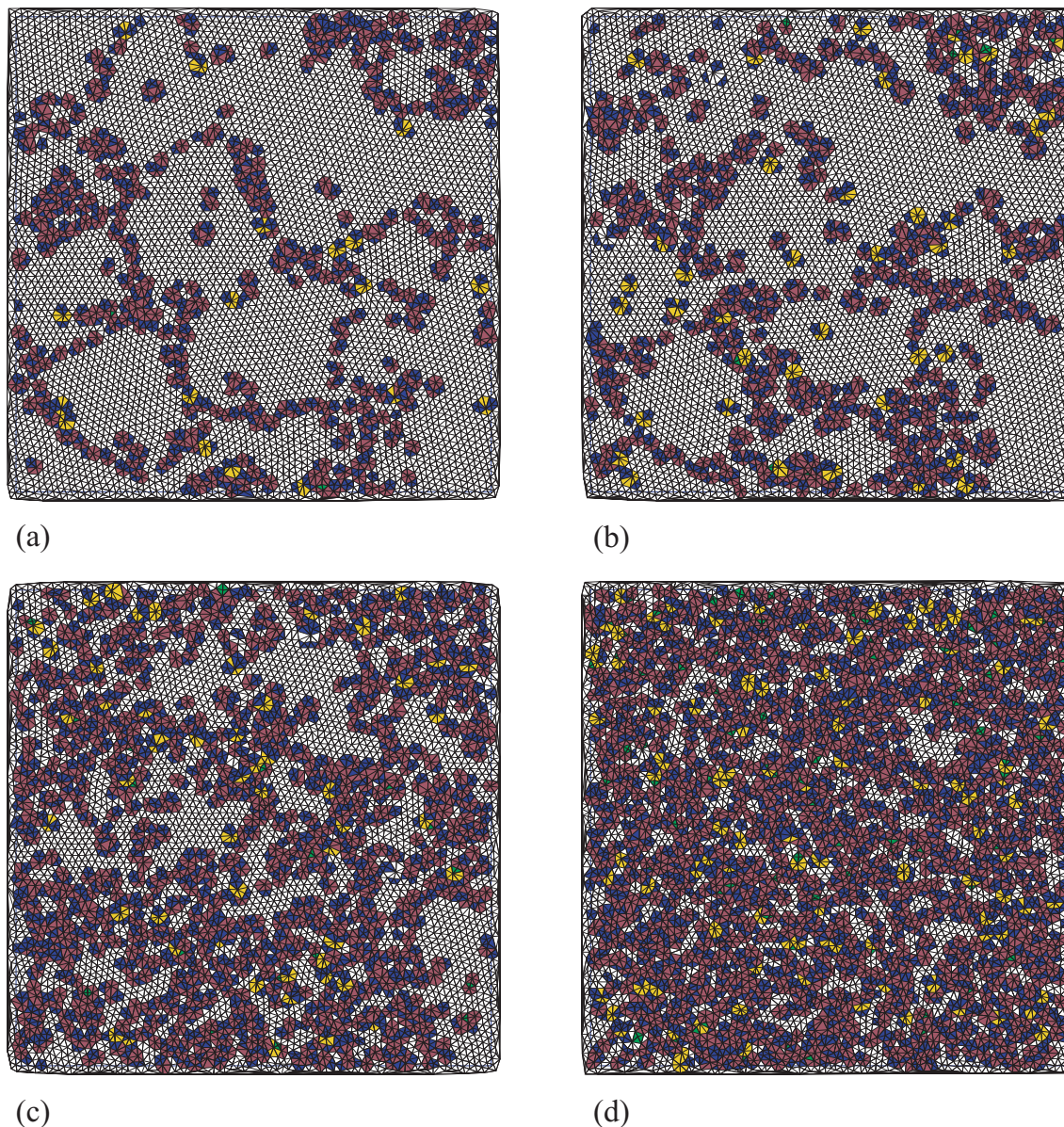


FIG. 10. (Color) Delauney triangulations for layers (a) one; (b) two; (c) three; and (d) four at $N=10.4$. Triangles surrounding sixfold-coordinated particles only have been left uncolored, while colored cells indicate a deviating coordination number: green for fourfold, blue for fivefold, brown for sevenfold, and yellow for eightfold-coordinated particles.

Furthermore, it can be seen when comparing Figs. 10(b) and 10(c) that the small crystal nuclei in the third layer are centered on top of the larger grains in the second layer, supporting the mechanism of epitaxial nucleation for layers two and further. Finally, for the fourth layer, typical liquid-like behavior is found, with rather few and small temporarily ordered regions.

D. Comparison to simulation results

In the preceding paragraphs an analysis was presented on the nature of the crystallization transition in a system of sedimenting charge-stabilized colloids with relatively large Peclet numbers, i.e., for strong gravitational field strength as compared to thermal forces. At some points a brief comparison with the work of Biben *et al.* was already made, which we will do more extensively below. The system of Biben *et al.* consisted of hard-sphere particles at a flat wall at a

constant areal density of 5.43 particles per squared hard-sphere diameter. These particles were subjected to an increasing gravitational field strength as expressed in the parameter $\alpha = mg\sigma/kT$, where m is the buoyant mass of the particles and σ is the hard-sphere diameter. A discontinuous jump was found to occur in both a layer-wise defined order parameter as well as the interlayer density for both the first and second layer when α was increased from 2.5 to 2.75. The order parameters for the third and fourth layer were, apart from a small jump for the third layer at $\alpha=2.75$, found to increase continuously with α . The range of increase of their order parameter for layers one to four is summarized in Table I.

One of the major differences between both systems is the use of hard-sphere particles versus the charge-stabilized silica particles used in this study. In order to quantitatively compare their results with ours, the mean-interparticle spac-

ing in a crystalline layer was calculated both from the volume fraction after complete sedimentation ($\varphi=0.31$; see Fig. 5) as well as from the position of the first peak in the layer-wise $g(r)$, and this value was taken as an effective hard-sphere diameter. For a similar system consisting of the same number of sedimented hard spheres, a volume fraction at the bottom of the sediment was calculated as $\varphi_{\text{HS}}=0.726$. With the volume fraction given above, this gives a measure of the softness of the interaction expressed as the actual particle radius over the effective hard-sphere radius of 1.33. For the hard-sphere diameter we now get $\sigma=1.340 \mu\text{m}$ and equal crystal plane number densities for both studies. As the buoyant mass of the model hard-sphere particles the actual particle buoyant mass in our experiments was taken, so that the softness of our interaction is treated by using an effective hard-sphere diameter with a lower particle density. This clearly means an oversimplification of the physical situation, but it does provide us with a situation where the contribution to the osmotic pressure of a close-packed layer at a certain α is similar in both studies. Thus, the results for increasing α can now be mapped on our results with increasing N , by comparing the respective osmotic pressures. Note that the constant areal density of $5.43/\sigma^2$ corresponds to a sediment thickness of 4.7 close-packed layers. The values for the resulting osmotic pressures at the values of α listed in Table I are given there as well. In this study the crystallization transition in the first layer was found to occur at an osmotic pressure of $\Pi=2.36 \times 10^{-2} \text{ N/m}^2$ (see Table I). This result is in remarkably good agreement with the values calculated on the basis of the results of Biben *et al.* Furthermore, the range in our experiment over which the bond-orientational order parameter shows its rise, roughly from $N=10.0$ to 11.2, gives an osmotic pressure difference of $\Delta\Pi=0.30 \times 10^{-2} \text{ N/m}^2$. The difference in osmotic pressure between α_{start} and α_{end} for crystallization of the first layer in the simulations is $\Delta\Pi=0.22 \times 10^{-2} \text{ N/m}^2$. Thus, the steepness of the rise in order parameter is very well reproduced in our experiments as well. The nature of the phase transition reported in the work of Biben *et al.*, namely a first-order discontinuous transition that occurs simultaneously in the first two layers, is also in correspondence with our experiment. For layers three and further, Biben and co-workers observed a continuous growth of the sediment as a function of α . If we look at the values for Π at the start and end of the transition for these layers (see Table I), it can be seen that these values are becoming increasingly off with respect to our experimental values. In our experimental situation with the number of particles in the sediment increasing continuously, it can be expected that the difference in sediment thickness between the crystallization of further layers reaches a constant value of $\Delta N=1$, corresponding to a value of the osmotic pressure that has to be reached for a liquid layer on a hexagonal substrate to crystallize. In fact, in Table I it can be seen that this situation is already almost reached at the fourth layer. Thus, we get an osmotic pressure of $\Pi=2.36 \times 10^{-2} \text{ N/m}^2$ at which a liquid layer of colloids crystallizes on a flat bottom wall, and a value of about $\Pi=1.98 \times 10^{-2} \text{ N/m}^2$ for epitaxial crystallization on a hexagonally ordered layer of colloids.

The above values can be compared with the value for the

pressure in a system of density-matched hard spheres at liquid–solid coexistence. The reduced pressure at coexistence is $\Pi^*=11.69=\Pi \cdot \sigma^3/kT$. With the effective hard-sphere radius used above ($\sigma=1.340 \mu\text{m}$), we get a value of $\Pi=1.83 \times 10^{-2} \text{ N/m}^2$, which is of the same order of magnitude and about 20% smaller than the values reported above for a system with gravity. Furthermore, Heni and Löwen recently determined the pressures for prefreezing of a hard-sphere liquid at a hard wall carrying a hexagonal wall pattern.^{15,16} They reported a value of $\Pi^*=8.53 \pm 0.12$, which gives $\Pi=1.34(\pm 0.01) \times 10^{-2} \text{ N/m}^2$ for our system. This gives a reduction of $\sim 73\%$ compared to the bulk coexistence pressure, compared to a reduction of $\sim 84\%$ in our system in gravity. However, a major difference between the two results is here not only the presence of gravity and the softness of the spheres, but the character of the wall pattern (fixed spheres versus Brownian spheres) as well.

The mechanism of epitaxial crystallization for layers two and further was confirmed in the structural analysis. However, the question remains whether the epitaxial crystallization in these layers proceeds via discontinuous first-order transitions or continuously. As we have not calculated the densities in layers three and four as a function of sediment thickness (actually, in order to do so the crystallization transition in these layers should be sampled more), a definite answer cannot be given. However, an indication about the nature of the transitions may be inferred from the behavior of the bond-orientational order parameter.

Above, the range of osmotic pressure over which the crystallization transition in the first layer takes place was found to be $\Delta\Pi=0.30 \times 10^{-2} \text{ N/m}^2$. For layer four the range in sediment thickness is from $N=11.2$ to about 12.75, which gives $\Delta\Pi=0.39 \times 10^{-2} \text{ N/m}^2$. This suggests that the nature of the phase transition in $\langle |\psi_6| \rangle$ does not change drastically, meaning that the growth of the sediment proceeds via layer-wise first-order transitions; however, more data on the growth of the sediment, preferentially by directly calculating the density or the relative ρ_z^{min} in the following layers, are needed. The indication mentioned above for discontinuous growth of the sediment is in contrast with the results of Biben. Furthermore, as mentioned above, there is also a discrepancy between the osmotic pressures for the crystallization of layers three and beyond which is remarkable in view of the good agreement of the results for the initial stage of crystallization. However, the system size in the direction perpendicular to the bottom wall is, in the study of Biben *et al.*, rather small, equivalent to only 4.7 crystal layers. Due to this fact, the range of the transition region for the third and the fourth layer as expressed in $\Delta\Pi$, which, as can be seen in Table I does not increase much from layer one to three, is smeared out considerably in α , as there are only a few particles on top. In fact, at this point the analogy between two systems fails: For a system like the lower layers with a sufficient amount of particles atop to well sample correlations between particles in the upper and lower parts, the increase of the osmotic pressure due to an increase in the number of particles can be well replaced by an increase of α . However, at a low amount of particles on top, their mean-field contribution to the osmotic pressure fails to describe the physical

situation with many particles higher in the sample. Here, the effect of increasing gravitational field strength cannot be mapped anymore onto our experimental situation of sedimenting colloids. This is illustrated by the fact that for the top part of the sediment in the simulations of Biben, the situation at a further increase of α finally yields a 2D system. A more complete test of the effect of increasing gravitational field strength with respect to thermal motion can be achieved by performing experiments on samples with a constant number density of spheres, but with different sphere sizes. Another approach could be the use of another, more controllable, external field than gravity, e.g., radiation pressure.²⁹

E. Equilibration during growth and the role of softness

One of the crucial aspects of the process of crystallization during sedimentation is the interplay between the time scales associated with both processes. Clearly, the conditions, i.e., the initial volume fraction, for sedimentation were chosen properly with respect to the nucleation kinetics, as our sediment did crystallize completely. However, this does not immediately imply that the sedimentation kinetics was sufficient for proper equilibration of the crystal structure. The crystalline end state in each layer was polycrystalline with a typical lateral grain size of approximately 40 μm wide, which results from the nucleation and growth mechanism in each layer. Time scales associated with the rearrangements necessary for a reduction of the polycrystallinity can be expected to be orders of magnitude larger than the time scales for nucleation and growth. In order to get some idea about the equilibration of the crystals in our sample, a structural analysis was performed and the same analysis was repeated starting from a twice-lower volume fraction. For a more detailed analysis of the stacking sequence of crystals grown by colloidal sedimentation, we refer to another publication.⁵⁴

The structure of the columnar crystallites two months after starting the experiments was of fcc type with a finite number of stacking faults of about 0.10 of the total number of layers in a crystallite. Redoing the sedimentation experiment at half the initial number was found to give a reduction of the number of incorrectly stacked layers to 0.06. The polycrystallinity was not observed to change. This indicates that the conditions that were used here were not sufficient to completely equilibrate our samples. We assume that longer equilibration will not change the character of the (first-order) phase transition as this is inherent in the nucleation- and growth stage of the process, but a substantial increase of equilibration times, for instance by lowering the volume fraction by one or two orders of magnitude, might reduce the polycrystallinity. This will increase the range of correlations in the radial distribution function $g(r)$ and the bond-orientational order correlation function $g_6(r)$, which is necessary for determining the decay rate of these functions, and thus the occurrence of an intermediate hexatic phase. In this way, for instance, the occurrence of an intermediate hexatic phase can be determined which was now obscured by the finite crystallite size. To conclude, we assume that the simul-

aneous transition of crystallization in the first two layers is the equilibrium behavior, even although the stacking sequence is not.

A final point of discussion is the interaction potential between the spheres in our system. The repulsive interaction between our spheres gives a final volume fraction of the crystalline end state of $\varphi=0.31$. For true hard-sphere particles this value would be 0.726, as calculated from osmotic and gravitational pressure at the bottom wall. However, the results of Biben *et al.* were, for as long as the mean-field approach in comparing the two systems holds, reproduced in very good agreement. Thus, despite the softness of the interactions, the nature of the phase transition and pressure at which the transition occurs are well reproduced assuming effective hard-sphere interactions. The softness can, however, be expected to play a large role in the kinetics of the transition. Recently, Gasser *et al.* reported real-space measurements probing colloidal nucleation in a system with a similar value for the crystal volume fraction.⁵ The values for the nucleation rates they reported are several order of magnitude higher than the theoretically expected values,³ which gives a strong indication of the effect of the softness of the interaction on the nucleation kinetics. Thus, performing similar experiments with true hard-sphere-like particles, for instance, sterically stabilized colloids in apolar solvent or a system similar to ours but with salt added to screen the repulsive interaction, may require a considerably lower initial volume fraction.

IV. CONCLUSIONS

A real-space analysis using confocal microscopy and fluorescent core-shell colloids was carried out on crystallization during particle sedimentation. Crystallization is preceded by layering of the liquid at the bottom of the sediment. Our model system consisted of 1- μm -diameter charged silica colloids, where the volume fraction in the crystal is on the order of $\varphi=0.31$, compared to a value of 0.726 that it would have in a hard-sphere system. The bottom-most liquid layer was found to undergo a first-order liquid–solid transition at a sediment thickness equivalent to 10.4 crystalline layers, which corresponds to an osmotic pressure of $\Pi=2.36 \times 10^{-2} \text{ N/m}^2$. The phase transition in the first layer was found to give rise to an increase in the values of the order parameters for the second layer, which as a consequence crystallizes simultaneously at a local osmotic pressure of $\Pi=2.13 \times 10^{-2} \text{ N/m}^2$. The simultaneous transition in the first two layers was found to be first order, as indicated by a direct evaluation of the relative interlayer density and the overall density in these two layers. The behavior of the bond-orientational order parameter displays a similar transition for these layers as for the bottom layers, but further research is needed in order to determine whether these successive transitions in each layer are of first order.

The crystallization process was found to proceed with the nucleation and subsequent growth of small crystallites, resulting in a polycrystalline end state. This polycrystallinity causes a sign inversion in the global bond-order correlation function beyond a typical crystallite size. As a consequence, the decay rate of this correlation function could not give any insight into the possible occurrence of an intermediate

hexatic phase between liquid and solid phases. However, if the hexatic phase occurs, the liquid–hexatic and hexatic–solid transitions are close.

In layers two and further, the formation of small crystal nuclei was found to occur on top of already crystallized or crystallizing grains, corresponding to epitaxial crystal growth. This gives rise to the lower osmotic pressure at crystallization compared to the first layer. The osmotic pressure for epitaxial nucleation could be inferred from fourth-layer crystallization at $\Pi = 1.98 \times 10^{-2} \text{ N/m}^2$.

Our results on the nature of the phase transition in the first two layers of the sediment are in good agreement with computer simulations that examined the phase transition in a hard-sphere system under increasing gravitational field strength. For the subsequent growth of the sediment, the results contradict the simulations, probably because of a different number of layers in the simulations as compared to our experiment.

ACKNOWLEDGMENTS

We would like to thank Didi Derks for performing exploratory measurements and Bela Mulder for a critical reading of the manuscript. We furthermore acknowledge helpful discussions with Daan Frenkel and Hartmut Löwen. This work is part of the research program of the “Stichting voor Fundamenteel Onderzoek der Materie (FOM),” which is financially supported by the “Nederlandse organisatie voor Wetenschappelijk Onderzoek (NWO).”

- ¹W. W. Wood and J. D. Jacobson, *J. Chem. Phys.* **27**, 1207 (1957).
- ²B. J. Alder and T. E. Wainwright, *J. Chem. Phys.* **27**, 1208 (1957).
- ³S. Auer and D. Frenkel, *Nature (London)* **409**, 1020 (2001).
- ⁴A. van Blaaderen and P. Wiltzius, *Science* **270**, 1177 (1995).
- ⁵U. Gasser, E. R. Weeks, A. Schofield, P. N. Pusey, and D. A. Weitz, *Science* **292**, 258 (2001).
- ⁶A. van Blaaderen and A. Vrij, *Langmuir* **8**, 2921 (1992).
- ⁷A. van Blaaderen, A. Imhof, W. Hage, and A. Vrij, *Langmuir* **8**, 1514 (1992).
- ⁸N. A. M. Verhaegh and A. van Blaaderen, *Langmuir* **10**, 1427 (1994).
- ⁹W. K. Kegel and A. van Blaaderen, *Science* **287**, 290 (2000).
- ¹⁰E. R. Weeks, J. C. Crocker, A. C. Levitt, A. Schofield, and D. A. Weitz, *Science* **287**, 627 (2000).
- ¹¹S. Dietrich, *Phase Transitions and Critical Phenomena* (Academic, London, 1988).
- ¹²D. H. Van Winkle and C. A. Murray, *J. Chem. Phys.* **89**, 3885 (1988).
- ¹³D. J. Courtemanche and F. van Swol, *Phys. Rev. Lett.* **69**, 2078 (1992).
- ¹⁴D. J. Courtemanche, T. A. Pasmore, and F. van Swol, *Mol. Phys.* **80**, 861 (1993).
- ¹⁵M. Heni and H. Löwen, *Phys. Rev. Lett.* **85**, 3668 (2000).
- ¹⁶M. Heni and H. Löwen, *J. Phys.: Condens. Matter* **13**, 4675 (2001).
- ¹⁷A. van Blaaderen, R. Ruel, and P. Wiltzius, *Nature (London)* **385**, 321 (1997).
- ¹⁸J. P. Hoogenboom, A. Yethiraj, A. K. van Langen-Suurling, J. Romijn, and A. van Blaaderen, *Phys. Rev. Lett.* **89**, 256104 (2002).
- ¹⁹W. B. Russel, D. A. Saville, and W. R. Schowalter, *Colloidal Dispersions* (Cambridge University Press, Cambridge, 1989).
- ²⁰J. X. Zhu, M. Li, R. Rogers, W. Meyer, R. H. Ottewill, W. B. Russel, and P. M. Chaikin, *Nature (London)* **387**, 883 (1997).
- ²¹J. E. G. J. Wijnhoven and W. L. Vos, *Science* **281**, 802 (1998).
- ²²M. Holgado, F. Garcia-Santamaria, A. Blanco *et al.*, *Langmuir* **15**, 4701 (1999).
- ²³P. V. Braun, R. W. Zehner, C. A. White, M. K. Weldon, C. Kloc, S. S. Patel, and P. Wiltzius, *Adv. Mater. (Weinheim, Ger.)* **13**, 721 (2001).
- ²⁴A. A. Zakhidov, R. H. Baughman, Z. Iqbal, C. X. Cui, I. Khayrullin, S. O. Dantas, I. Marti, and V. G. Ralchenko, *Science* **282**, 897 (1998).
- ²⁵A. Blanco, E. Chomski, S. Grachtchak *et al.*, *Nature (London)* **405**, 437 (2000).
- ²⁶K. E. Davis, W. B. Russel, and W. J. Glantschnig, *Science* **245**, 507 (1989).
- ²⁷T. Biben, R. Ohnesorge, and H. Löwen, *Europhys. Lett.* **28**, 665 (1994).
- ²⁸K. Zahn, R. Lenke, and G. Maret, *Phys. Rev. Lett.* **82**, 2721 (1999).
- ²⁹M. Brunner, C. Bechinger, W. Strepp, V. Lobaskin, and H. H. van Grönberg, *Europhys. Lett.* **58**, 926 (2002).
- ³⁰K. J. Strandburg, *Bond-Orientational Order in Condensed Matter Systems* (Springer, New York, 1992).
- ³¹J. M. Kosterlitz and D. J. Thouless, *J. Phys. Chem.* **6**, 1181 (1973).
- ³²J. M. Kosterlitz and D. J. Thouless, *J. Phys. Chem.* **7**, 1046 (1974).
- ³³B. I. Halperin and D. R. Nelson, *Phys. Rev. Lett.* **41**, 121 (1978).
- ³⁴A. P. Young, *Phys. Rev. B* **19**, 1855 (1979).
- ³⁵A. Jaster, *Phys. Rev. E* **59**, 2594 (1999).
- ³⁶M. A. Bates and D. Frenkel, *Phys. Rev. E* **61**, 5223 (2000).
- ³⁷P. Bladon and D. Frenkel, *Phys. Rev. Lett.* **74**, 2519 (1995).
- ³⁸A. H. Marcus and S. A. Rice, *Phys. Rev. Lett.* **77**, 2577 (1996).
- ³⁹C. A. Murray and D. H. Van Winkle, *Phys. Rev. Lett.* **58**, 1200 (1987).
- ⁴⁰R. E. Kusner, J. A. Mann, J. Kerins, and A. J. Dahm, *Phys. Rev. Lett.* **73**, 3113 (1994).
- ⁴¹P. Karnchanaphanurach, B. H. Lin, and S. A. Rice, *Phys. Rev. E* **61**, 4036 (2000).
- ⁴²J. L. Barrat, T. Biben, and J. P. Hansen, *J. Phys.: Condens. Matter* **4**, L11 (1992).
- ⁴³R. Piazza, T. Bellini, and V. Degiorgio, *Phys. Rev. Lett.* **71**, 4267 (1993).
- ⁴⁴M. A. Rutgers, J. H. Dunsmuir, J. Z. Xue, W. B. Russel, and P. M. Chaikin, *Phys. Rev. B* **53**, 5043 (1996).
- ⁴⁵C. A. Murray, in *Bond-Orientational Order in Condensed Matter Systems*, edited by K. J. Strandburg (Springer, New York, 1992), pp. 137–215.
- ⁴⁶H. Giesche, *J. Eur. Ceram. Soc.* **14**, 205 (1994).
- ⁴⁷J. C. Crocker and D. G. Grier, *J. Colloid Interface Sci.* **179**, 298 (1996).
- ⁴⁸IDL (Interactive Data Language) is a product of Research Systems Inc. and is especially suited for and widely used in the processing of array-based information.
- ⁴⁹H. Löwen, *Phys. Rev. E* **53**, R29 (1996).
- ⁵⁰K. Zahn and G. Maret, *Phys. Rev. Lett.* **85**, 3656 (2000).
- ⁵¹M. M. Hurley and P. Harrowell, *Phys. Rev. E* **52**, 1694 (1995).
- ⁵²H. Löwen, T. Palberg, and R. Simon, *Phys. Rev. Lett.* **70**, 1557 (1993).
- ⁵³A discontinuous increase in the density accompanied by a sharp decrease to zero in the interlayer density as shown by Biben *et al.* would show up more pronounced if the ratio of the two is considered.
- ⁵⁴J. P. Hoogenboom, D. Derks, P. Vergeer, and A. van Blaaderen, *J. Chem. Phys.* **117**, 11320 (2002).